Bare-nucleus astrophysical factor of the ^{3}He$(d, p)^4$He reaction via the "Trojan horse" method

M. La Cognata,[1,2] C. Spitaleri,[1,2] A. Tumino,[1,2] S. Typel,[3] S. Cherubini,[1,2] L. Lamia,[1,2] A. Musumarra,[1,2] R. G. Pizzone,[1,2] A. Rinollo,[1,2] C. Rolfs,[4] S. Romano,[1,2] D. Schürmann,[4] and F. Strieder[4]

[1]*Dipartimento di Metodologie Fisiche e Chimiche per l'Ingegneria - Università di Catania, Catania, Italy*

[2]*Laboratori Nazionali del Sud - INFN, Catania, Italy*

[3]*Gesellschaft für Schwerionenforschung mbH, Darmstadt, Germany*

[4]*Ruhr-Universität, Bochum, Germany*

(Received 22 February 2005; revised manuscript received 28 July 2005; published 27 December 2005)

The ^{3}He$(d, p)^4$He reaction has been studied from $E_{\text{c.m.}} = 600$ keV down to astrophysical energies by means of the "Trojan horse" method using the ^{6}Li$(^3$He$, p\alpha)^4$He three-body reaction at $E_{\text{lab}} = 5$ and 6 MeV. Coincidence spectra were measured in kinematic conditions favoring the quasifree ^{3}He + ^{2}H process. The bare astrophysical factor $S_b(E)$ for the ^{3}He$(d, p)^4$He reaction was extracted from the three-body cross section in the modified plane-wave Born approximation. Comparison with the S_b extrapolation from the free two-body data is presented. The independent estimate of the screening potential as obtained with the present work seems to confirm the theoretical adiabatic limit.

DOI: 10.1103/PhysRevC.72.065802 PACS number(s): 26.20.+f, 21.10.Pc, 24.50.+g, 25.70.Hi

I. INTRODUCTION

Measurements of bare-nucleus cross sections for the ^{3}He$(d, p)^4$He, ^{3}H$(d, n)^4$He, ^{2}H$(d, p)^3$H, and ^{2}H$(d, n)^3$He fusion reactions, at ultra-low energies, are of interest in pure and applied physics. These reactions are involved in homogeneous and inhomogeneous primordial nucleosynthesis [1–4], i.e., in the production of ^{2}H, ^{3}He, ^{4}He, and ^{7}Li nuclear ashes from the early universe. These nuclei are used to extract information on the baryon density of the universe.

Moreover, their importance is connected with the understanding of the electron screening effect which appears to be significantly larger than could be accounted for from the adiabatic limit [5,6]. It prevents one from directly measuring the astrophysically relevant bare-nucleus cross section. The extraction of the electron screening potential provides important information on the role of electrons in favoring deuteron-induced as well as tritium-induced reactions, which are used in fusion reactors in the same energy range as that relevant to nuclear astrophysics ($kT \approx 1$ to 100 keV). The hope is that in the near future, fusion reactors can supply the necessary energy for industrial and commercial use.

Recently, a new investigation of ^{2}H$(d, p)^3$H and ^{3}He$(d, p)^4$He reactions at ultra-low energies was carried out via the "Trojan horse" method (THM) [7,8]. In the present paper, the THM is applied to the ^{3}He$(d, p)^4$He reaction, which was investigated by selecting the quasifree (QF) contribution from the ^{6}Li$(^3$He$, p\alpha)^4$He three-body process. The evidence of this reaction mechanism, which for the present case was pointed out in previous works [9–11], is a preliminary and necessary condition for the applicability of the THM [12–15] to the indirect extraction of the two-body cross sections. The ^{3}He$(d, p)^4$He two-body reaction also shows a resonant behavior at $E_{\text{c.m.}} = 0.21$ MeV (well below the Coulomb barrier) due to an excited state ($E^* = 16.66$ MeV) in the compound system, i.e., the ^{5}Li nucleus. The observation of such a resonance in the excitation function extracted with the THM would prove to be an important result of this measurement.

II. BARE-NUCLEUS CROSS SECTION

A. Electron screening

Astrophysical reactions between charged particles are difficult to measure directly at the relevant Gamow energy because of the exponential drop in the probability of penetrating the Coulomb barrier. In addition, ultra-low energy measurements are affected by the screening effect of atomic electrons [16], which hinders the direct determination of the bare cross section $\sigma_b(E)$, the relevant input needed for astrophysical purposes. The screening effect leads to an enhancement of $\sigma_b(E)$ by the factor

$$f_{\text{lab}}(E) = \sigma_s(E)/\sigma_b(E) \approx \exp(\pi \eta U_e/E), \tag{1}$$

where $\sigma_s(E)$ is the cross section of shielded nuclei and U_e is the electron screening potential [5,6,16].

The bare cross section $\sigma_b(E)$ in the Gamow energy region is determined by an extrapolation of experimental data taken at energies where electron screening effects are negligible, e.g., $E/U_e \geqslant 100$. Usually the extrapolation is performed on the bare-nucleus astrophysical factor $S_b(E)$, a much smoother function of energy, defined as

$$S_b(E) = E\sigma_b(E)\exp(2\pi\eta), \tag{2}$$

where $\exp(2\pi\eta)$ is the inverse of the Gamow factor (η being the Sommerfeld parameter) which removes the dominant energy dependence of $\sigma_b(E)$ caused by the barrier penetration.

A screening effect is also present in stellar plasmas where free electrons cluster around the positively charged ions at a characteristic Debye-Hückel radius depending on the stellar plasma's temperature and density. However, the enhancement factor in the plasma is different from that observed in the laboratory. It can be expressed as

$$f_{\text{pl}}(E) = \sigma_{\text{pl}}(E)/\sigma_b(E) \approx \exp(\pi \eta U_{\text{pl}}/E), \tag{3}$$

with a plasma screening potential U_{pl}.

Corrections for plasma conditions are applied to the bare cross section; hence, a measurement of the screening potential

U_e under laboratory conditions can eventually provide a better understanding of the screening potential $U_{\rm pl}$ in the plasma.

For many reactions studied so far ([6] and references therein), experimental U_e values were found to be much larger than the upper theoretical estimates, i.e., the adiabatic limits, given as the difference between the electron binding energies of the separate atoms in the entrance channel and that of the composite final system [5,6,16]. This disagreement is not explained yet, and clearly it does not help in understanding screening effects under astrophysical conditions.

A weak point in the laboratory approach—and thus in the deduced U_e value—is the need for an assumption about the energy dependence of $\sigma_b(E)$ at ultra-low energies. To avoid the extrapolation, alternative experimental methods for determining $\sigma_b(E)$ appear highly desirable.

B. Indirect methods

In recent years, a number of indirect methods have been introduced as a complementary way of measuring cross sections of astrophysical relevance.

The Coulomb dissociation [17–19] and asymptotic normalization coefficient [20–28] methods can only be used to extract astrophysical $S(E)$ factors for radiative capture reactions. In contrast, the Trojan horse method (THM) [7,8,12–15,29–35,35–39] is applicable to nuclear reactions where no photons are involved.

Despite its being an indirect approach, the THM offers the possibility of extracting a *measured* bare $S(E)$ factor as opposed to that extrapolated, albeit with theoretical guidance, from direct data. Therefore, it offers an independent way of determining electron screening potentials.

The THM has already been applied to several reactions of astrophysical relevance [2–4,40] such as ^{7}Li$(p,\alpha)^4$He, ^{6}Li$(d,\alpha)^4$He, ^{6}Li$(p,\alpha)^3$He, ^{9}Be$(p,\alpha)^6$Li, ^{11}B$(p,\alpha_o)^8$Be, ^{6}Li$(n,t)^4$He, and ^{2}H$(d,p)^3$H connected with fundamental astrophysical problems [2–4,40]. These reactions were studied through the ^{2}H(^{7}Li,$\alpha\alpha$)n [13,30,31,33,34,41], ^{6}Li(^{6}Li,$\alpha\alpha$)^{4}He [12,35,36], ^{2}H(^{6}Li,α^3He)n [38,39], ^{2}H(^{9}Be,$^6Li\alpha$)n [42, 43],^{2}H(^{11}B,$\alpha_o{}^8$Be)n [15,44], and ^{2}H(^{6}Li,tp)^{4}He [7,45] three-body reactions, respectively.

III. TROJAN HORSE METHOD: BASIC FEATURES

The application of the quasifree (QF) mechanism to the study of reactions at astrophysical energies [46] originates from previous studies of the QF mechanism at very low energies [47–56]. A QF reaction $A + a(= x + s) \rightarrow C + c + s$ can be described in the framework of the impulse approximation (IA) by using a polar diagram (Fig. 1), where only the first term of the Feynman series is retained. The first pole describes the virtual breakup of the target nucleus a into the clusters x and s, where s is considered to be spectator to the $A + x \rightarrow C + c$ reaction which takes place in the second pole.

In the THM, the $A + a$ reaction occurs at a c.m. energy E_{Aa} above the Coulomb barrier. However, the quasifree $A + x$ process can take place even at very low sub-Coulomb energies

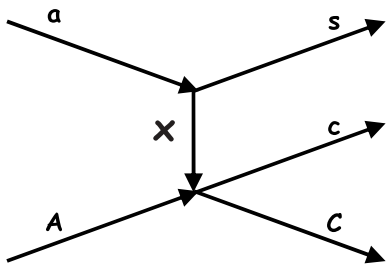

FIG. 1. Pole diagram representing the $A(a, cC)s$ quasifree reaction.

E_{Ax} by appropriately selecting kinematic conditions, where the x-s binding energy compensates for the $A + a$ relative motion. The nuclei C and c are detected at the so-called quasifree angles [15,35]. The reaction of astrophysical interest takes place at the *quasifree two-body energy* given by

$$E_{\rm QF} = E_{Ax} - B_{x\text{-}s}, \tag{4}$$

which is equivalent to the expression given in Ref. [37].

A cutoff in the momentum distribution, which is related to the Fermi motion of s inside the Trojan horse nucleus a, fixes the range of energies E_{Ax} around the quasifree two-body energy accessible for the reaction of astrophysical relevance. Since the Trojan horse method effectively removes the Coulomb barrier for the system A-x, the interaction takes place within the nuclear region and is thus unaffected by either the Coulomb suppression or the electron screening effects.

Following theoretical approaches based on the IA, the experimental three-body cross section can be expressed in terms of the two-body cross section of interest, the momentum distribution of the spectator and a kinematic factor. In the present work, the approach based on a modified plane-wave Born approximation (MPWBA) [32,35–39] was applied, where the factorization of the three-body cross section is retained. This approach employs the surface approximation in order to derive an expression of the three-body T-matrix element in terms of the S-matrix elements of the astrophysical two-body reaction. In addition, Coulomb distortion is introduced in the two-body channel and off-energy-shell effects are fully included. The MPWBA triple differential cross section is given by

$$\frac{d^3\sigma}{dE_C d\Omega_C d\Omega_c} = {\rm KF}\,|W(\vec{Q}_{Bs})|^2\,\frac{v_{Cc}}{v_{Ax}} \times \sum_l T_l C_l \frac{d\sigma_l}{d\Omega}(Cc \rightarrow Ax), \tag{5}$$

where the interference from different partial waves l is neglected. The quantity $d\sigma_l/d\Omega$ represents the on-shell two-body cross section for the reaction $C + c \rightarrow A + x$ in partial wave l, whose Coulomb suppression at low energies is compensated for by the presence of the inverse penetration factor

$$T_l(k_{Ax}R) = G_l^2(k_{Ax}R) + F_l^2(k_{Ax}R). \tag{6}$$

The momentum amplitude $W(\vec{Q}_{Bs})$ is connected to the wave function of the TH nucleus a in momentum space and is

given by

$$W(\vec{Q}_{Bs}) = -\left(B_{x\text{-}s} + \frac{\hbar^2 Q_{Bs}^2}{2\mu_{xs}}\right) \times \langle \exp(i\vec{Q}_{Bs}\cdot\vec{r}_{xs})\Phi_x\Phi_s|\Phi_a\rangle. \quad (7)$$

The argument $\vec{Q}_{Bs}$ corresponds to the momentum transfer to the spectator s. KF is a kinematic factor,

$$\mathrm{KF} = \frac{\mu_{Aa}m_C}{(2\pi)^5\hbar^7}\frac{p_C p_c^3}{p_{Aa}}\left[\left(\frac{\vec{p}_{Bs}}{\mu_{Bs}} - \frac{\vec{p}_{Cc}}{m_c}\right)\cdot\frac{\vec{p}_c}{p_c}\right]^{-1}, \quad (8)$$

in obvious notation for (relative) momenta and (reduced) masses, where B denotes the $C + c$ system and C_l is a constant. The expression (5) strongly resembles the factorization of the cross section in the plane-wave impulse approximation (PWIA) [57] further corrected for the Coulomb penetration. The *a priori* inclusion of Coulomb and off-shell effects is indeed the essential feature of the present approach. The appearance of the constant factor C_l and the employed approximations prevent the absolute value of the two-body cross section from being extracted. However, the absolute magnitude of the cross section can be derived from a scaling to direct data available at higher energies.

IV. EXPERIMENTAL SETUP

The ^{6}Li(^{3}He,$p\alpha$)^{4}He experiment was performed at the Dynamitron Tandem Laboratorium in Bochum, Germany. The 4 MV tandem accelerator provided a ^{3}He beam at energies $E = 5$ and 6 MeV with a spot size on target of approximately 1 mm and a typical intensity of 10 nA.

The beam was delivered onto an isotopically enriched lithium fluoride target (^{6}Li $\approx 95\%$). The detection setup consisted of two pairs of coincidence telescopes arranged symmetrically at opposite sides of the beam direction. Each telescope consisted of a 20 μm (500 μm) ΔE detector and a 500 μm (1000 μm) position sensitive detector (PSD) as E detector, the thicker detectors being used for proton identification.

The angular position of each pair was optimized in order to detect the outgoing α particle and proton in coincidence at the quasifree angles [15,35]. The selected angular ranges, $9^\circ \leqslant \theta_\alpha \leqslant 23^\circ$ for α particles and $136^\circ \leqslant \theta_p \leqslant 156^\circ$ for protons, correspond to kinematic conditions where the momentum of the undetected α particle (i.e., the spectator) ranges from -100 to 100 MeV/c. This ensures that the bulk of the quasifree contributions of the breakup process falls within the experimental phase-space region. This also enables us to cross-check the method because it is possible to study the reaction mechanism inside and outside the region where the quasifree contribution is expected to dominate.

Energy and position signals of the PSDs were processed by standard electronic chains together with the delay between the time signals for each coincidence event and sent to the acquisition system for the on-line monitoring and data storing of the experiment.

V. DATA ANALYSIS

A number of steps are involved in the analysis of data before the two-body cross section of astrophysical relevance can be extracted. These steps include (a) identification of events due to the three-body reaction of interest; (b) identification of events due to the QF mechanism; (c) subtraction of spurious events arising from mechanisms other than the QF breakup, if present; (d) extraction of the two-body cross section from the measured three-body one and normalization to direct data; (e) extraction of the astrophysical $S(E)$ factor for bare nuclei; and (f) determination of the screening potential. Each of these steps is described in detail in the following paragraphs, together with a number of tests to cross-check the validity of the results obtained so far.

A. PSD calibration and identification of ^{6}Li(^{3}H,αp)^{4}He reaction

Energy calibration of each PSD was performed by means of a standard three-peak α source and data from elastic scattering of ^{3}He on ^{1}H and ^{12}C at beam energies of about 5 and 6 MeV. For the higher energy region, the ^{12}C(^{3}He,p)^{14}N, ^{6}Li(^{3}He,^{4}He)^{5}Li, and ^{6}Li(^{3}He,p)^{8}Be reactions were considered instead.

The overall energy resolution was found to be about 2% for both the 5.48 MeV α-source peak and the elastic scattering of ^{3}He on ^{12}C or ^{1}H.

Angular calibration was achieved by using grids with equally spaced slits placed in front of each PSD during preliminary runs of the experiment in order to establish a position-angle correspondence. From the identification of the ^{3}He + ^{6}Li two-body reactions, the angular resolution was found to be about 0.3°.

After the identification of the coincident α and proton and the assumption of mass 4 for the undetected third particle, the locus of events in the E_α vs E_p plane was reconstructed (Fig. 2). It was found to be in agreement with the expected kinematic locus for the ^{6}Li(^{3}He,$p\alpha$)^{4}He three-body reaction.

The Q-value spectrum for the selected coincidence events is reported in Fig. 3. A prominent peak observed around $E = 17$ MeV is in very good agreement with the Q-value (16.88 MeV) for the three-body reaction of interest. Only events inside this peak were considered for further analysis.

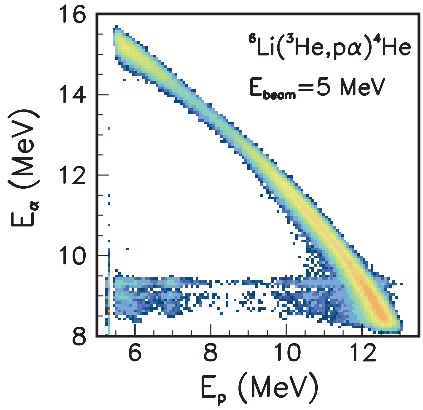

FIG. 2. (Color online) E_α vs E_p correlation plot. The kinematic locus for the ^{6}Li(^{3}He,$p\alpha$)α reaction is clearly visible.

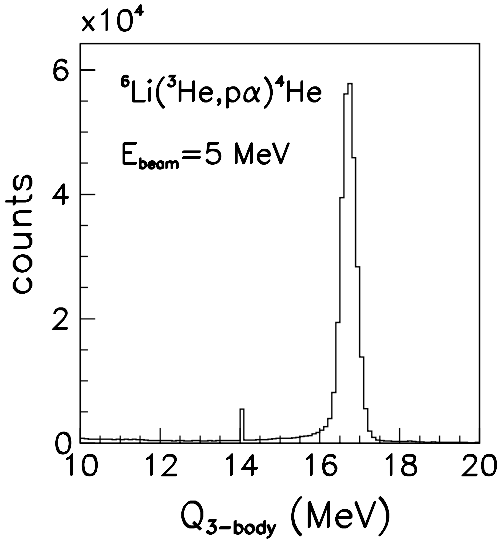

FIG. 3. Three-body Q-value spectrum. A dominant peak centered around 17 MeV can be seen clearly.

B. Experimental evidence of the quasifree mechanism

1. Relative energy two-dimensional plots

After selecting events corresponding to the ^{6}Li(^{3}He,$p\alpha$)^{4}He reaction, one has to determine the contribution of the QF process to the overall p-α coincidence yield. Indeed, the analysis of the experimental results is in general complicated by the presence of other reaction mechanisms feeding the same particles in the final state, e.g., sequential decay (SD) and direct breakup. In the large range of the available proton and α energies, the following SD processes may contribute (see Fig. 4):

$$^6\mathrm{Li}(^3\mathrm{He},\, p)^8\mathrm{Be}^*, \qquad ^8\mathrm{Be}^* \rightarrow \alpha + \alpha, \tag{9}$$

$$^6\mathrm{Li}(^3\mathrm{He},\, \alpha)^5\mathrm{Li}^*, \qquad ^5\mathrm{Li}^* \rightarrow p + \alpha, \tag{10}$$

through excited states of ^{8}Be and ^{5}Li. In order to preliminarily study the nature of the events belonging to the kinematic locus for the ^{6}Li(^{3}He,$p\alpha$)^{4}He reaction, relative energies for any two of the three final particles were calculated. Figures 5(a) and 5(b) show coincidence events projected onto the α-α vs p-α and p-α vs p-α relative energy planes.

A locus at $E_{\alpha\text{-}\alpha} = 3.0$ MeV, corresponding to the 2^+ state of ^{8}Be at 3.0 MeV of excitation energy, is clearly shown in Figs. 5(a) and 5(b). No other loci seem to be present in any other two-dimensional plot. From such a comprehensive relative energy two-dimensional plot analysis, it can be stated that the ^{6}Li(^{3}He,$p\alpha$)^{4}He reaction mainly proceeds through formation of an intermediate ^{8}Be excited nucleus, in agreement with previous investigations [11,58]. This SD contribution from the 3.0 MeV state of ^{8}Be has been disentangled from the QF mechanism as described in the following sections.

2. Study of angular correlation spectra

A way to discriminate between SD and QF events is through an angular correlation analysis of the data. Coincidence data were projected onto the proton energy axis E_p at a fixed angle for one of the two particles and different angles for the other particle. Figures 6(a)–6(c) show examples of the angular correlation spectra at a beam energy of 6 MeV for

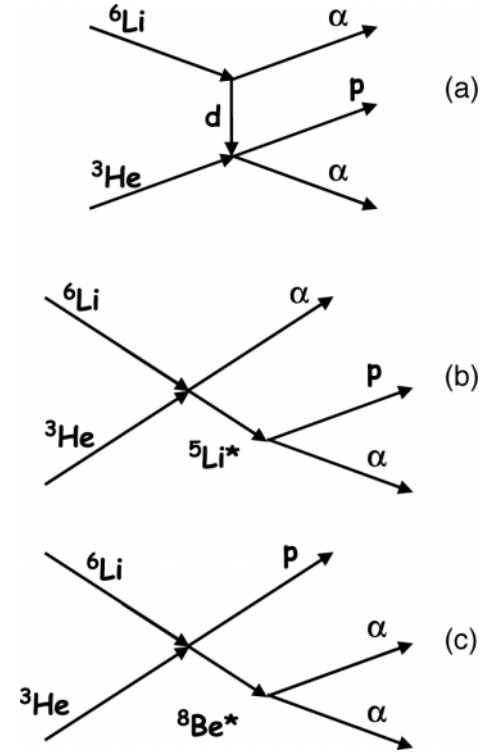

FIG. 4. Simplified scheme for the ^{6}Li(^{3}He,$p\alpha$)α quasifree reaction (a) and two possible competitive channels, ^{6}Li(^{3}He,α)^{5}Li*($p\alpha$) (b) and ^{6}Li(^{3}He,p)^{8}Be*($\alpha\alpha$) (c) sequential decays, with the same particles in the exit channel.

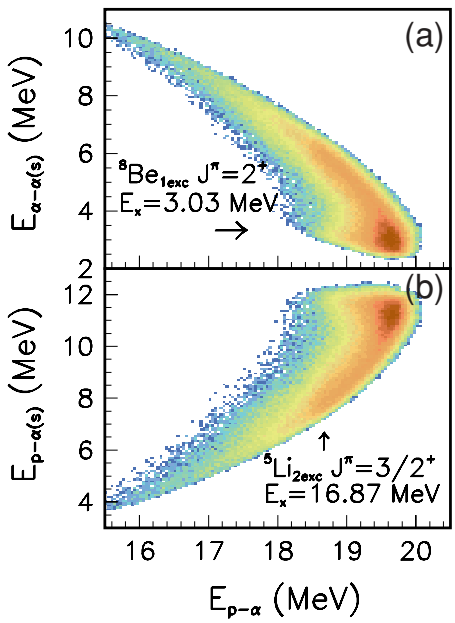

FIG. 5. (Color online) $E_{\alpha\text{-}\alpha}$ vs $E_{p\text{-}\alpha}$ (a) and $E_{p\text{-}\alpha}$ vs $E_{p\text{-}\alpha}$ (b) relative energy correlation plots.

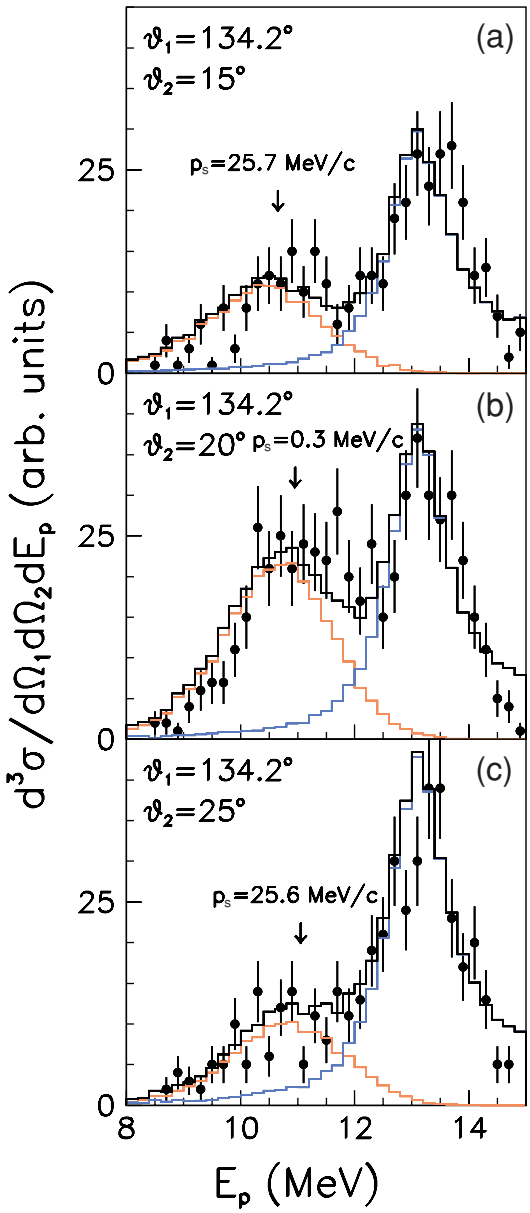

FIG. 6. (Color online) Typical angular correlation spectra at a beam energy of 6 MeV. Coincidence data are projected onto the E_p variable for $\theta_p = 134.2^\circ$ and $\theta_\alpha = 15^\circ$–25°.

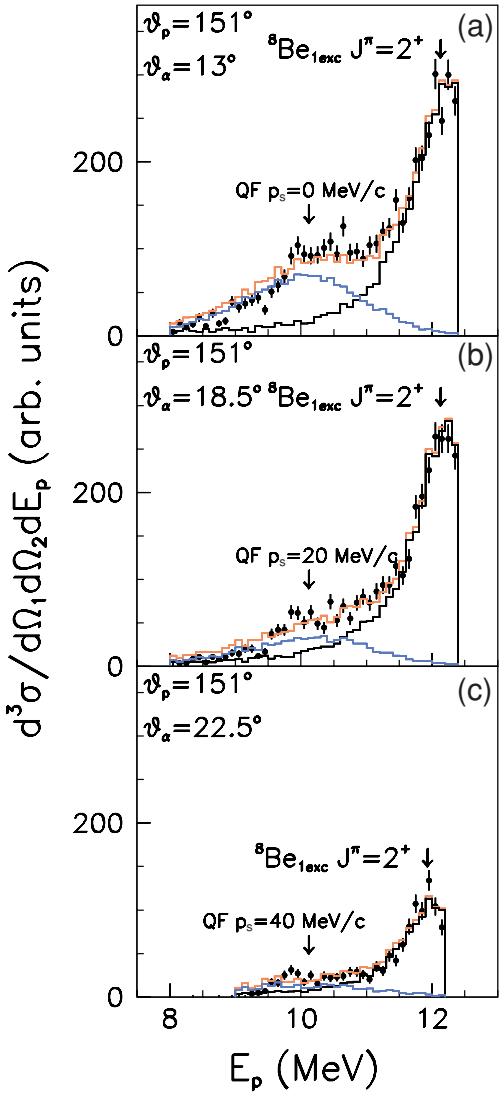

FIG. 7. (Color online) Typical angular correlation spectra at a beam energy of 5 MeV. Coincidence data are projected onto the E_p variable for $\theta_p = 151^\circ$ and $\theta_\alpha = 13^\circ$–22.5°.

a proton angle $\theta_p = 134.2^\circ$ and angles for the α particle $\theta_\alpha = 15^\circ$, 20°, and 25°. Since the momentum distribution of the p-α system in ^{6}Li has a maximum for $p_\alpha = 0$ MeV/c, the feature expected for a quasifree reaction is a coincidence yield attaining a maximum when the momentum of the α particle, indicated in the following as p_s, approaches zero. The $(\theta_p, \theta_\alpha)$ angles corresponding to this condition represent the so-called quasifree angles.

The arrows in Figs. 6(a)–6(c) mark the position where the energy E_s (or equivalently the momentum p_s) of the undetected α particle takes its minimum value for a given angle pair (i.e., the quasifree angles). In agreement with the expected QF behavior, an enhancement in the coincidence yield is observed for the quasifree angles [6(b)], which decreases when moving away from this condition [6(a) and 6(c)]. At higher energies, a large increase of the coincidence yield not correlated with p_s values shows up. This is due to SD events from the 3.0 MeV state of ^{8}Be. Similar results have been obtained for other quasifree angle pairs.

The same considerations apply to Figs. 7(a)–7(c), showing typical angular correlation spectra at a beam energy of 5 MeV, for a fixed proton angle $\theta_p = 151^\circ$ and angles for the α particle of $\theta_\alpha = 13^\circ$, 18°, and 22.5°.

3. *Data as a function of the α momentum p_s*

In order to better investigate which p_s momentum region is populated in the ^{8}Be* SD contribution, two-dimensional plots were reconstructed for all coincidence events, giving the p-α (or equivalently α-α) relative energy vs p_s momentum in the whole angular range covered by the detectors. The results shown in Figs. 8(a) and 8(b) indicate that the ^{8}Be decay mainly contributes in the region of $|p_s| \geqslant 30$ MeV/c. However, a tail

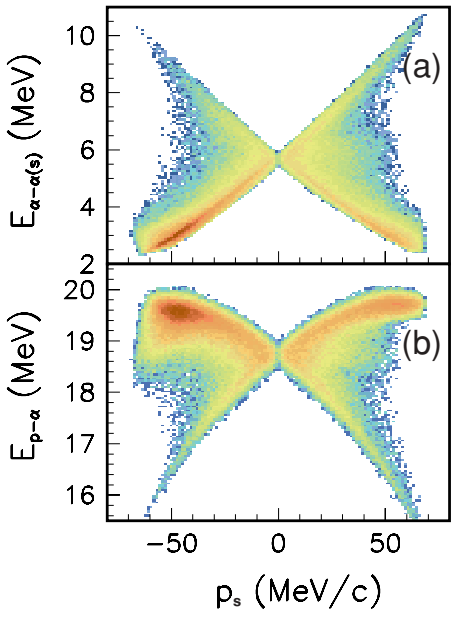

FIG. 8. (Color online) Two-dimensional spectra for $E_{\alpha\text{-}\alpha}$ vs p_s (a) and $E_{p\text{-}\alpha}$ vs p_s (b). The contribution from the sequential decay of the first excited level in ^{8}Be is clearly visible.

is also present at lower $|p_s|$ values, corresponding to the QF region. Thus, a separation between the two contributions is required as described below.

4. Subtraction of SD contribution from the 3.0 MeV state of ^{8}Be

In order to disentangle the QF coincidence data from the ^{8}Be* SD contribution, the following procedure was employed. The first step was to select the kinematic regions where the QF mechanism contribution is expected to dominate, i.e., around the QF angles. Coincidence events for each pair of QF angles were then projected onto the $E_{\alpha\text{-}\alpha}$ relative energy axis as shown in Fig. 9. Here the resonant contribution from the 3.0 MeV excited state in ^{8}Be is evident. The arrows on these figures mark the $E_{\alpha\text{-}\alpha}$ energies to which peaks due to resonances in ^{8}Be and ^{5}Li may contribute. The energy regions where the minimum momentum of the spectator particle is expected are marked with arrows. The vertical bars represent statistical errors on the three-body cross section.

The ^{8}Be SD contribution was estimated by fitting the resonant behavior with a Breit-Wigner function with level parameters $E_0 = 3.0$ MeV and $\Gamma = 1.5$ MeV from [59], and subtracted from the total events in the spectrum. A weight function was derived dividing the resulting $E_{\alpha\text{-}\alpha}$ spectrum by the original one. It was used to disentangle the SD contribution in the other observables.

5. Analysis of the α momentum distribution in ^{6}Li

An observable which turns out to be very sensitive to the reaction mechanism is the shape of the experimental momentum distribution of the spectator. In order to reconstruct the experimental p_s distribution, the energy sharing method [49] was applied for each pair of coincidence QF angles, selecting ^{3}He-d relative energy windows of 100 keV.

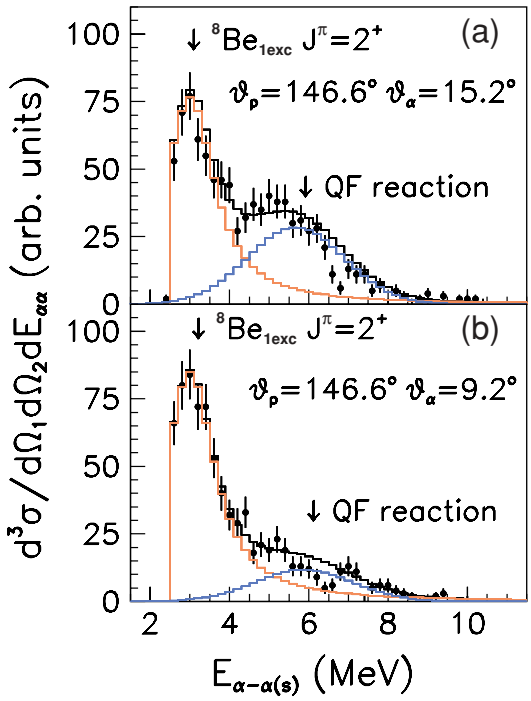

FIG. 9. (Color online) Spectra of the $E_{\alpha\text{-}\alpha}$ relative energy for two different angular pairs. An incoherent sum of SD and QF contributions closely reproduces the energy behavior.

After subtracting the ^{8}Be contribution, the weighted coincidence yield was divided by the kinematic factor, leaving a quantity proportional to the product between the α momentum distribution and the differential $^3\mathrm{He}+{}^2\mathrm{H}$ two-body cross section [15]. However, within such restricted energy windows, the differential two-body cross section of the $^3\mathrm{He}-{}^2\mathrm{H}$ reaction can be considered almost constant.

Thus, the quantity defined above and reported in Fig. 10 represents the experimental p_s momentum distribution in arbitrary units for the ^{6}Li(^{3}He,αp)^{4}He channel. Data were

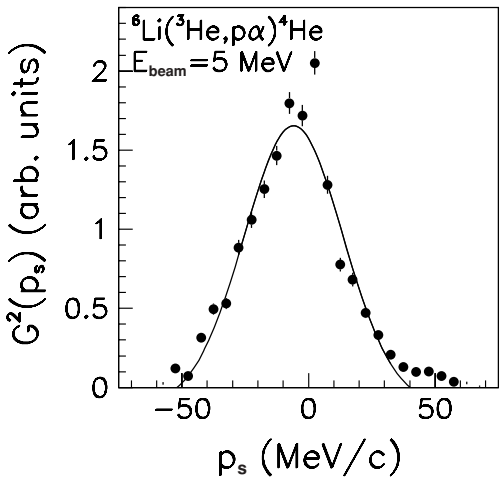

FIG. 10. Experimental momentum distribution (solid dots) compared with the theoretical one given in terms of a Hankel function (solid line). See text for details.

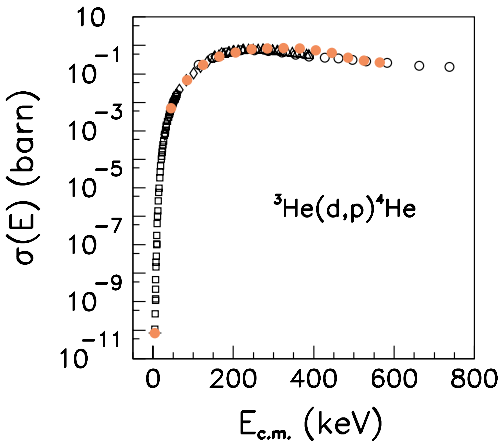

FIG. 11. (Color online) THM cross section for the ^{3}He(d, p)^{4}He reaction (solid dots) compared with direct data from [61–63,65].

projected in 5 MeV/c bins with error bars including statistical errors only. The extracted experimental momentum distribution (Fig. 10) was then compared with the theoretical one (dashed curve), given in terms of a Hankel function in momentum space

$$|G(p_s)|^2 = \frac{N}{\left(k_s^2+\beta^2\right)^2}\left[\frac{\sin(k_s R_c)}{k_s}+\frac{\cos(k_s R_c)}{\beta}\right]^2, \quad (11)$$

where $k_s = (p_s - p_0)/\hbar$, R_c is the cutoff radius, and $\beta = (2\mu B_{\alpha\text{-}d}/\hbar^2)^{1/2}$, with the α-d binding energy $B_{\alpha\text{-}d}$ of ^{6}Li and their reduced mass μ.

A fit of experimental data using Eq. (11) with parameters $R_c = (10.4 \pm 0.3)$ fm, $N = (5.82 \pm 0.11) \times 10^{-4}$ and $p_0 = (-5.9 \pm 0.4)$ MeV/c is shown in Fig. 10 in arbitrary units. The theoretical distribution reproduces quite well the shape of the experimental data. Its full width at half maximum is (43.6 ± 0.5) MeV/c, in agreement with the value expected from the literature for the α-d system in ^{6}Li [60].

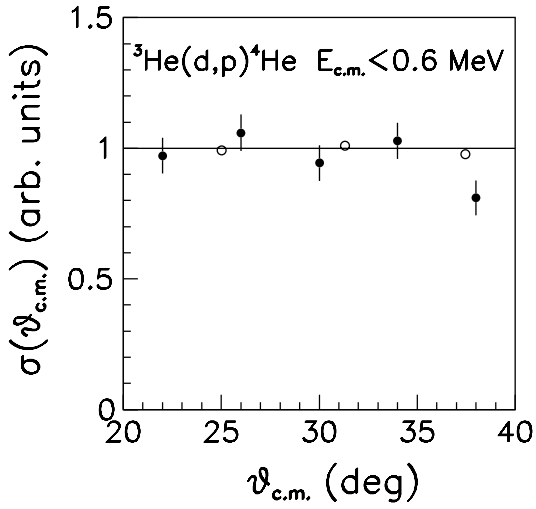

FIG. 12. THM angular distribution for $0 \leqslant E_{\text{c.m.}} \leqslant 600$ keV (solid dots), compared with direct data from [65].

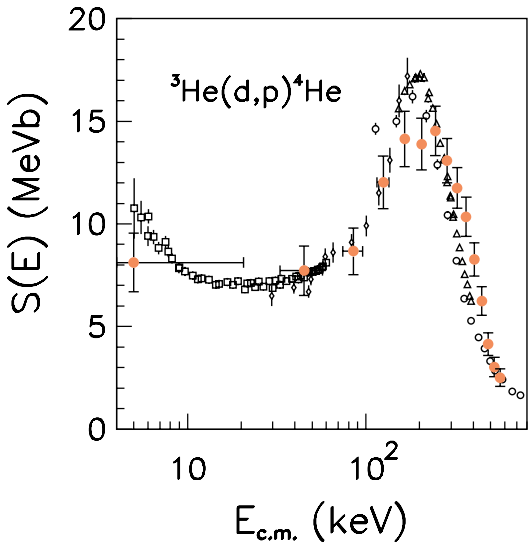

FIG. 13. (Color online) Astrophysical $S(E)$ factor for the ^{3}He(d, p)^{4}He reaction (solid circles) compared with direct data from [61] (open squares), [62] (open triangles), [65] (open circles), and [63] (open diamonds).

Having disentangled the QF contribution from a significant component due to a contaminant SD process, further data analysis was performed only on the subset of events caused by the QF mechanism alone.

C. From the QF coincidence data to the indirect two-body cross section

For the extraction of the indirect two-body excitation function, only coincidence events with $0 \leqslant p_s \leqslant 10$ MeV/c were considered. The weighted coincidence yield was projected onto the $E_{^3\text{He-}d}$ variable ($E_{^3\text{He-}d} = E_{\alpha\text{-}p} - Q_{\text{two-body}}$ in post-collision prescription [15,39]) with a 40 keV bin

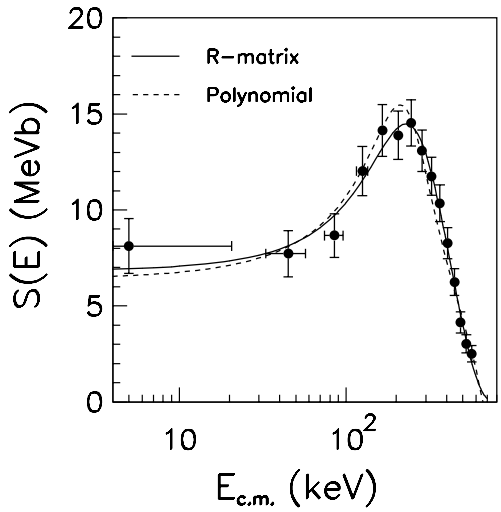

FIG. 14. Astrophysical $S(E)$ factor for the ^{3}He(d, p)^{4}He reaction: experimental points as in Fig. 13. Solid line shows the behavior of the bare-nucleus $S(E)$ factor from the R-matrix calculation; dashed line represents the result of the polynomial fit using Eq. (13).

TABLE I. Astrophysical S factor for the ^{3}He$(d, p)^4$He reaction. Energy, energy uncertainty, S factor, and corresponding error are reported. See text for detailed discussion.

E (keV)	ΔE (keV)	S_b (MeV b)	ΔS_b (MeV b)
5	16	8.1	1.4
45	12	7.7	1.2
85	11	8.7	1.1
125	10	12.0	1.3
165	8	14.1	1.3
205	7	13.9	1.2
245	7	14.5	1.2
285	6	13.1	1.1
325	6	11.7	1.0
365	6	10.3	0.9
405	6	8.3	0.8
445	6	6.2	0.7
485	6	4.1	0.5
525	6	3.0	0.5
565	7	2.5	0.4

after integrating over the $E_{\alpha\text{-}\alpha}$ variable within each bin. All coincidence spectra, each corresponding to a given pair of $(\theta_p, \theta_\alpha)$ quasifree angles, were then summed up to provide the relative energy $E_{^3\text{He}\text{-}d}$ three-body cross section in arbitrary units, free of the ^{8}Be SD contribution. The experiment was simulated by a Monte Carlo calculation based on the MPWBA with the momentum distribution given in Eq. (11). The geometric efficiency of the experimental setup as well as the detection thresholds of the detectors were fully taken into account.

Following the prescription of Eq. (5), the two-body cross-section $d\sigma_0/d\Omega_{\text{c.m.}}$ was derived by dividing the selected three-body experimental coincidence yield by the result of the Monte Carlo calculation [15]. The resonant contribution from the 16.66 MeV state of ^{5}Li in the $^4\text{He} + p$ two-body channel is clearly observed. It could not be seen in the relative energy two-dimensional plot analysis (Figs. 5(a) and 5(b), before background subtraction) because of the strong presence of the ^{8}Be SD.

Normalization of the direct excitation data was performed in the resonant region between 100 and 600 keV. Figure 11 shows the final two-body cross section as obtained in the present work (solid symbols) together with the direct data (open symbols) [61–65] used for the normalization procedure. The very good agreement between the two data sets confirms the usefulness of the MPWBA analysis in correctly describing the studied process at low energies.

D. Angular distributions

An additional cross-check was performed by comparing the angular distributions obtained in this work with those available from direct experiments. For the investigated three-body reaction, the emission angle of the α particle in the α-p center-of-mass system can be calculated according to the relation [52]

$$\theta_{\text{c.m.}} = \arccos \frac{(\vec{v}_d - \vec{v}_{^3\text{He}}) \cdot (\vec{v}_p - \vec{v}_\alpha)}{|\vec{v}_d - \vec{v}_{^3\text{He}}||\vec{v}_p - \vec{v}_\alpha|}, \qquad (12)$$

where the vectors $\vec{v}_d$, $\vec{v}_{^3\text{He}}$, $\vec{v}_p$, and $\vec{v}_\alpha$ are the velocities of the transferred deuteron, the ^{3}He nucleus, and the outgoing proton and α particle, respectively. These quantities can be calculated from their corresponding momenta in the laboratory system, where, according to the quasifree assumption [57], the momentum of the transferred particle is equal and opposite to that of the spectator (here the α particle).

The angular distribution test was performed on the same data set as selected for the extraction of the two-body cross section. Results (in arbitrary units) are shown in Fig. 12, with error bars including both statistical and systematic errors. The obtained angular distributions were then normalized and compared with the direct data from [65] in the populated angular region. The solid line of Fig. 12 shows the behavior of the direct angular distributions [65]. Again, the good agreement between the two data sets can be taken as evidence of the validity of the MPWBA.

VI. RESULTS

A. Bare-nucleus astrophysical factor

The procedure to derive the $S(E)$ factor from our data employs the usual definition (2). Figure 13 shows the extracted $S(E)$ factor compared with direct data [61–63,65]. The results for the ^{3}He$(d, p)^4$He reaction in the form of the $S(E)$ factor are summarized in Table I.

Vertical error bars include statistical and normalization errors as well as the error coming from the subtraction of the SD contribution. This error ranges from 10 to 20%, the largest value corresponding to the lowest energy region where the SD contribution dominates. The horizontal bars reflect the energy resolution in the $E_{\text{c.m.}}$ variable, about 15 keV, determined by means of standard formulas starting from the experimental uncertainties affecting energy and angle of emission of each ejectile. In spite of the large error bars, the data sets show the same energy trend above $E_{\text{c.m.}} \approx 20$keV and also the ^{5}Li resonance is well reproduced. The discrepancy observed at energies $E_{\text{c.m.}} \leqslant 20$ keV is due to the electron screening effect,

TABLE II. Parameters for the THM bare-nucleus $S_b(E)$ factor using Eq. (13): (1) refers to the fit including all the THM data, while in (2) the lowest energy point is left out. For completeness the previous value reported in [8] is also shown.

S_0 (MeV b)	S_1 (b)	S_2 (MeV^{-1} b)	W_{res} (MeV^3 b)	$S_b(E=0)$ (MeV b)	Ref.
2.70	14.3	−30	0.2	6.0 ± 1.8	[8]
3.30	12.67	−28.8	0.202	6.4 ± 1.3	Present work (1)
2.01	15.91	−30.9	0.218	5.4 ± 1.4	Present work (2)

TABLE III. R-matrix parameters for the THM bare-nucleus $S_b(E)$ factor. All THM data points are considered (total $\chi^2 = 4.66$).

Level	E_r (MeV)	γ_1 (MeV$^{1/2}$)	γ_2 (MeV$^{1/2}$)
1	13.817	0.5251	1.6087
2	17.064	0.1443	0.4232
3	30.000[a]	4.1390	2.6871

[a]Kept constant in the fit.

which is no longer negligible for the direct data. As in our previous preliminary analysis [8] performed with only a minor part of the selected events, the THM data were fitted with the expression

$$S_b(E) = S_0 + S_1\, E + S_2\, E^2 + \frac{W_{\rm res}}{(E-\Gamma_0)^2 + \Gamma_0^2/4}, \quad (13)$$

where the Lorentz function describes the resonant behavior at $E_0 = 0.21$ MeV with resonance width $\Gamma_0 = 0.27$ MeV [59]. The values of the fitting parameters S_0, S_1, S_2, and $W_{\rm res}$ are reported in Table II leading to a bare-nucleus zero-energy $S(E)$ factor of $S_b(0) = (6.4 \pm 1.3)$ MeV b, with a total χ^2 of 15.21.

The quoted uncertainty accounts for a statistical error of 3%, an error of 19% arising from the subtraction of the SD contribution and a systematic error of 5% due to the normalization procedure. In the present analysis, the $S(E)$ factor was extracted with better statistics and with an improved uncertainty of 20% instead of the previous 30%.

In addition, following the suggestion in [66] a two-level R-matrix fit was performed on the THM data assuming two $\frac{3}{2}^+$ states with $l_i = 0$ in the ^{3}He + ^{2}H channel and $l_f = 2$ in the ^{4}He + p channel. A channel radius of 5 fm and a background resonance at 30 MeV were assumed. The total χ^2 of this two-level calculation is 4.66. The level parameters for the calculation are given in Table III. This more realistic approach provided an $S_b(0) = (6.8 \pm 1.4)$ MeV b, where the error accounts for the same sources of uncertainty as described before, but with a statistical error of 5%.

The results of both fits are reported in Fig. 14 as solid (R-matrix) and dashed (polynomial fit) lines, superimposed onto the THM points already shown in Fig. 13.

Furthermore, the fit of the THM data were repeated by leaving out the lowest energy point. The new polynomial fit (see Table II for fitting parameters) as well as the R-matrix calculation (see Table IV for level parameters) provide much smaller zero-energy bare-nucleus $S(E)$ factors,

TABLE IV. R-matrix parameters for the THM bare-nucleus $S_b(E)$ factor. The lowest energy point is left out of the calculation (total $\chi^2 = 3.42$).

Level	E_r (MeV)	γ_1 (MeV$^{1/2}$)	γ_2 (MeV$^{1/2}$)
1	13.878	2.6305	1.2895
2	16.693	0.4803	0.2435
3	30.000[a]	5.7210	2.9270

[a]Kept constant in the fit.

TABLE V. R-matrix $S_b(0)$ values obtained from previous calculations on the direct data. In the last row the extrapolation of [63] is also reported.

$S_b(E=0)$ (MeV b)	Ref.
6.70	[62]
6.11	[66]
5.9 ± 0.3	[67]
5.84	[68]
6.51	[63]

$S_b(0) = (5.4 \pm 1.4)$ and $S_b(0) = (5.1 \pm 1.1)$ MeV b, respectively, in disagreement with the previous direct estimates. Although the lowest energy point is affected by a large error, its influence on the final result of the fitting procedures appears not to be negligible.

Within experimental errors, our $S_b(0)$ estimates agree with the values from previous R-matrix calculations [62,66,67] as well as from direct extrapolation [63] (see Table V).

B. Electron screening potential

In order to determine the electron screening potential U_e for the ^{3}He$(d,\, p)^4$He reaction, a fit of the screened $S(E)$ factor from direct data [61] can be performed using the bare-nucleus $S(E)$ factor parametrizations as determined via the THM in the present work. Here the relationship

$$S_{\rm screen}(E) = S_b(E) \exp(\pi \eta U_e / E) \quad (14)$$

is used, where the screening potential energy U_e is left as a free parameter. The results of the fit to the direct data [61] are shown in Fig. 15 together with the parametrizations for the THM bare-nucleus $S(E)$ factor. The fit yields $U_e = (155 \pm 34)$ eV, in agreement within the experimental errors with the values reported in [62,69–71], but lower than the estimates of [61] (see Table VI).

The more precise R-matrix parametrization provides a U_e value of (126 ± 29) eV. Both estimates are consistent, and the one from the R-matrix fit appears to agree also with the theoretical adiabatic limit.

TABLE VI. Estimates for the electron screening potential U_e. In (1) the employed bare nucleus $S(E)$ factor is given by Eq. (13); in (2) it is derived from the R-matrix fit (all THM data are included in the procedures). The theoretical adiabatic limit for U_e is 115 eV.

Reaction	$U_e^{\rm exp}$ (eV)	Ref.
^{3}He$(d,\, p)\alpha$	219 ± 7	[61]
^{3}He$(d,\, p)\alpha$	177 ± 29	[62]
^{3}He$(d,\, p)\alpha$	170 ± 28	[62]
^{3}He$(d,\, p)\alpha$	130 ± 8	[69]
^{3}He$(d,\, p)\alpha$	186 ± 9	[70]
^{3}He$(d,\, p)\alpha$	120 ± 10	[71]
^{6}Li$(^3$He$,p\alpha)\alpha$	180 ± 40	[8]
^{6}Li$(^3$He$,p\alpha)\alpha$	155 ± 34	Present work (1)
^{6}Li$(^3$He$,p\alpha)\alpha$	126 ± 29	Present work (2)

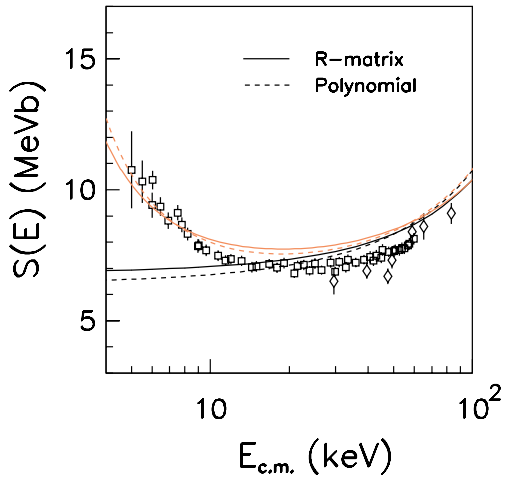

FIG. 15. (Color online) Screened $S(E)$ factors (red lines) from Eq. (14) together with the parametrizations for the THM bare-nucleus $S(E)$ factor (black lines). Solid lines refer to the R-matrix calculation; dashed lines correspond to the polynomial fit with Eq. (13).

VII. CONCLUSIONS

The indirect study of the ^{3}He(d, p)^{4}He reaction was performed from $E_{\text{c.m.}} = 600$ keV down to astrophysical energies applying the THM to the ^{6}Li(^{3}He,$p\alpha$)^{4}He three-body breakup process.

The results show that the three-body channel is mainly populated via an SD process involving the 3.0 MeV level of ^{8}Be, and only a small number of events are fed through the QF reaction mechanism off the ^{2}H in ^{6}Li. The ^{8}Be SD mainly leaves the α particles with momentum values larger than 30 MeV/c. But also within the region of nearly zero spectator momentum ($p_\alpha \leqslant 10$ MeV/c), a tail of this process is present. It had to be disentangled from the QF events, thus causing a strong reduction of the statistics.

The bare-nucleus $S(E)$ factor extracted in the present work fairly agrees with the behavior of direct data in the region where screening effects are negligible. In order to estimate the $S_b(0)$ parameter, a polynomial fit using Eq. (13) and an R-matrix calculation were performed on the THM data. Furthermore, they were employed to extract the U_e screening potential. In particular, the more realistic R-matrix calculation provides a U_e value that is still in agreement within experimental errors with previous results [62,69–71], but also confirms the theoretical adiabatic limit. However, additional investigations to put these conclusions on firmer grounds require the study of the low-energy region with more statistics while also using a different three-body reaction leading to the same two-body process. A good candidate might be the ^{3}H(^{3}He,αp)n reaction, involving the ^{3}H nucleus as the TH and a neutron as the spectator. The advantage of this reaction would be that of removing the SD contribution from ^{8}Be*, the largest source of uncertainty in this case. Moreover, such an alternative reaction would also enable the investigation of the role of the Trojan horse bound state in the THM. A feasibility study is currently underway.

ACKNOWLEDGMENTS

The authors would like to thank P. Corvisiero for fruitful suggestions during the preparation of the experiment and M. G. Pellegriti for the Collaboration during the experiment. They warmly acknowledge M. Aliotta and M. Gulino for their valuable help in the final drafting of this paper.

[1] G. Steigmann, Annu. Rev. Nucl. Part. Sci. **29**, 313 (1079).
[2] C. J. Copi, D. N. Schramm, and M. S. Turner, Science **267**, 192 (1995).
[3] D. N. Schramm and M. S. Turner, Rev. Mod. Phys. **70**, 303 (1998).
[4] R. A. Malaney and G. S. Mathews, Phys. Rep. **229**, 145 (1993).
[5] G. Fiorentini, R. W. Kavanagh, and C. Rolfs, Z. Phys. **350**, 289 (1995).
[6] F. Streider, C. Rolfs, C. Spitaleri, and P. Corvisiero, Naturwissenschaften **88**, 461 (2001).
[7] A. Rinollo, S. Romano, C. Spitaleri, C. Bonomo, S. Cherubini, A. Del Zoppo, P. Figuera, M. La Cognata, A. Musumarra, M. G. Pellegriti, R. G. Pizzone, C. Rolfs, D. Schürmann, F. Streider, S. Tudisco, and A. Tumino, Nucl. Phys. **A758**, 146 (2005).
[8] M. La Cognata, A. Musumarra, C. Spitaleri, A. Tumino, C. Bonomo, S. Cherubini, P. Figuera, L. Lamia, M. G. Pellegriti, A. Rinollo, R. G. Pizzone, C. Rolfs, S. Romano, D. Schürmann, F. Strieder, S. Tudisco, and S. Typel, Nucl. Phys. **A758**, 98 (2005).
[9] S. Barbarino, M. Lattuada, F. Riggi, C. Spitaleri, C. M. Sutera, and D. Vinciguerra, Nuovo Cimento A **53**, 327 (1979).
[10] M. Lattuada, F. Riggi, C. Spitaleri, D. Vinciguerra, C. M. Sutera, and A. Pantaleo, Nuovo Cimento A **71**, 429 (1982).
[11] M. Zadro, Đ. Miljanić, M. Lattuada, F. Riggi, and C. Spitaleri, Nucl. Phys. **A474**, 373 (1987).
[12] S. Cherubini, V. N. Kondratyev, M. Lattuada, C. Spitaleri, Đ. Miljanić, M. Zadro, and G. Baur, Astrophys. J. **457**, 855 (1996).
[13] C. Spitaleri, M. Aliotta, S. Cherubini, M. Lattuada, Dj. Miljanić, S. Romano, N. Soić, M. Zadro, and R. A. Zappalà, Phys. Rev. C **60**, 055802 (1999).
[14] C. Spitaleri, S. Cherubini, A. Del Zoppo, A. Di Pietro, P. Figuera, M. Gulino, M. Lattuada, Đ. Miljanić, A. Musumarra, M. G. Pellegriti, R. G. Pizzone, C. Rolfs, S. Romano, S. Tudisco, and A. Tumino, Nucl. Phys. **A719**, 99 (2003).
[15] C. Spitaleri, L. Lamia, A. Tumino, R. G. Pizzone, S. Cherubini, A. Del Zoppo, P. Figuera, M. La Cognata, A. Musumarra, M. G. Pellegriti, A. Rinollo, C. Rolfs, S. Romano, and S. Tudisco, Phys. Rev. C **69**, 055806 (2004).
[16] H. J. Assenbaum, K. Langanke, and C. Rolfs, Z. Phys. A **327**, 461 (1987).
[17] G. Baur and H. Rebel, J. Phys. G **20**, 1 (1994) and references therein.

[18] G. Baur and H. Rebel, Annu. Rev. Nucl. Part. Sci. **46**, 321 (1996).
[19] G. Baur, K. Hencken, and D. Trautmann, Prog. Part. Nucl. Phys. **51**, 487 (2003).
[20] X. Tang, A. Azhari, C. A. Gagliardi, A. M. Mukhamedzhanov, F. Pirlepesov, L. Trache, R. E. Tribble, V. Burjan, V. Kroha, and F. Carstoiu, Phys. Rev. C **67**, 015804 (2003).
[21] C. A. Gagliardi, A. Azhari, V. Burjan, F. Carstoiu, V. Kroha, A. M. Mukhamedzhanov, A. Sattarov, X. Tang, L. Trache, and R. E. Tribble, Eur. Phys. J. A **13**, 227 (2002).
[22] A. M. Mukhamedzhanov, C. A. Gagliardi, and R. E. Tribble, Phys. Rev. C **63**, 024612 (2001).
[23] A. Azhari, V. Burjan, F. Carstoiu, C. A. Gagliardi, V. Kroha, A. M. Mukhamedzhanov, F. M. Nunes, X. Tang, L. Trache, and R. E. Tribble, Phys. Rev. C **63**, 055803 (2001).
[24] A. M. Mukhamedzhanov and R. E. Tribble, Phys. Rev. C **59**, 3418 (1999).
[25] C. A. Gagliardi, R. E. Tribble, A. Azhari, H. L. Clark, Y. W. Lui, A. M. Mukhamedzhanov, A. Sattarov, L. Trache, V. Burjan, J. Cejpek, V. Kroha, S. Piskor, and J. Vincour, Phys. Rev. C **59**, 1149 (1999).
[26] A. Azhari, V. Burjan, F. Carstoiu, H. Dejbakhsh, C. A. Gagliardi, V. Kroha, A. M. Mukhamedzhanov, L. Trache, and R. E. Tribble, Phys. Rev. Lett. **82**, 3960 (1999).
[27] A. M. Mukhamedzhanov, H. L. Clark, C. A. Gagliardi, Y. W. Lui, L. Trache, R. E. Tribble, H. M. Xu, V. Cejpek , V. Burjan, V. Kroha, and F. Carstoiu, Phys. Rev. C **56**, 1302 (1997).
[28] H. M. Xu, C. A. Gagliardi, R. E. Tribble, A. M. Mukhamedzhanov, and N. K. Timofeyuk, Phys. Rev. Lett. **73**, 2027 (1994).
[29] G. Baur, Phys. Lett. **B178**, 135 (1986).
[30] G. Calvi, S. Cherubini, M. Lattuada, S. Romano, C. Spitaleri, M. Aliotta, G. Rizzari, M. Sciuto, R. A. Zappalà, V. N. Kondratyev, Đ. Miljanić, M. Zadro, G. Baur, O. Yu. Goryunov, and A. A. Shvedov, Nucl. Phys. **A621**, 139c (1997).
[31] C. Spitaleri, M. Aliotta, P. Figuera, M. Lattuada, R. G. Pizzone, S. Romano, A. Tumino, C. Rolfs, L. Gialanella, F. Strieder, S. Cherubini, A. Musumarra, Đ. Miljanić, S. Typel, and H. H. Wolter, Eur. Phys. J. A **7**, 181 (2000).
[32] S. Typel and H. Wolter, Few Body Syst. **29**, 7 (2000).
[33] M. A. Aliotta, C. Spitaleri, M. Lattuada, A. Musumarra, R. G. Pizzone, A. Tumino, C. Rolfs, and F. Strieder, Eur. Phys. J. A **9**, 435 (2000).
[34] M. Lattuada, R. G. Pizzone, S. Typel, P. Figuera, Đ. Miljanić, A. Musumarra, M. G. Pellegriti, C. Rolfs, C. Spitaleri, and H. H. Wolter, Astrophys. J. **562**, 1076 (2001).
[35] C. Spitaleri, S. Typel, R. G. Pizzone, M. Aliotta, S. Blagus, M. Bogovac, S. Cherubini, P. Figuera, M. Lattuada, M. Milin, Đ. Miljanic, A. Musumarra, M. G. Pellegriti, D. Rendic, C. Rolfs, S. Romano, N. Soic, A. Tumino, H. H. Wolter, and M. Zadro, Phys. Rev. C **63**, 055801 (2001).
[36] A. Musumarra, R. G. Pizzone, S. Blagus, M. Bogovac, P. Figuera, M. Lattuada, M. Milin, Đ. Miljanic, M. G. Pellegriti, D. Rendic, C. Rolfs, N. Soic, C. Spitaleri, S. Typel, H. H. Wolter, and M. Zadro, Phys. Rev. C **64**, 068801 (2001).
[37] S. Typel and G. Baur, Ann. Phys. (NY) **305**, 228 (2003).
[38] A. Tumino, C. Spitaleri, S. Cherubini, A. Di Pietro, P. Figuera, M. Lattuada, A. Musumarra, M. G. Pellegriti, R. G. Pizzone, S. Romano, C. Rolfs, S. Tudisco, and S. Typel, Nucl. Phys. **A718**, 499c (2003).
[39] A. Tumino, C. Spitaleri, A. Di Pietro, P. Figuera, M. Lattuada, A. Musumarra, M. G. Pellegriti, R. G. Pizzone, S. Romano, C. Rolfs, S. Tudisco, and S. Typel, Phys. Rev. C **67**, 065803 (2003).
[40] L. Piau and S. Turck-Chieze, Astrophys. J. **566**, 419 (2002).
[41] M. Zadro, Đ. Miljanic, C. Spitaleri, G. Calvi, M. Lattuada, and F. Riggi, Phys. Rev. C **40**, 181 (1989).
[42] C. Spitaleri, in Proceedings of 5th Rencontres du Vietnam Particle Physics and Astrophysics, Hanoi, 2004 (to be published).
[43] S. Romano, L. Lamia, C. Li, C. Spitaleri, S. Cherubini, M. Gulino, M. La Cognata, A. Musumarra, R. G. Pizzone, S. Tudisco, and A. Tumino, in press on Eur. Phys. J. A.
[44] S. Romano, C. Spitaleri, L. Lamia, A. Tumino, R. G. Pizzone, S. Cherubini, A. Del Zoppo, P. Figuera, M. Gulino, M. La Cognata, A. Musumarra, M. G. Pellegriti, A. Rinollo, and S. Tudisco, Nucl. Phys. **A738**, 406 (2004).
[45] A. Tumino, C. Spitaleri, C. Bonomo, S. Cherubini, P. Figuera, M. Gulino, M. La Cognata, A. Musumarra, M. G. Pellegriti, R. G. Pizzone, A. Rinollo, and S. Romano, Eur. Phys. J. A **25**, 649 (2005).
[46] C. Spitaleri, in *Problems of Fundamental Modern Physics II* (World Scientific, Singapore, 1990), pp. 21–35.
[47] Đ. Milianić, T. Zabel, R. B. Lambert, and G. C. Phylips, Nucl. Phys. **A215**, 221 (1973).
[48] M. Furic, R. K. Cole, H. H. Forster, C. C. Kim, D. Y. Park, J. Rucker, H. Spizer, and C. N. Weddell, Phys. Lett. **B39**, 629 (1972).
[49] J. Kasagi, T. Nakagawa, N. Sekine, and T. Tohei, Nucl. Phys. **A239**, 233 (1975).
[50] A. K. Jain, J. Y. Grossiodor, M. Chevalier, P. Gaillard, A. Guichard, M. Gusakow, and J. P. Pizzi, Nucl. Phys. **A216**, 519 (1973).
[51] Đ. Milianić, J. Hudomalj, G. S. Mutchler, E. Andrade, and G. C. Phylips, Phys. Lett. **B50**, 330 (1974).
[52] I. Slaus, R. G. Allas, L. Beach, R. O. Bondelid, E. L. Petersen, J. M. Lambert, P. A. Taedo, and A. Molyle, Nucl. Phys. **A286**, 67 (1977).
[53] N. Arena, D. Vinciguerra, F. Riggi, and C. Spitaleri, Nuovo Cimento **45**, 405 (1978).
[54] M. Lattuada, F. Riggi, C. Spitaleri, D. Vinciguerra, S. Micheletti, and A. Pantaleo, Nuovo Cimento **62**, 165 (1981).
[55] M. Lattuada, F. Riggi, C. Spitaleri, D. Vinciguerra, C. M. Sutera, and A. Pantaleo, Nuovo Cimento **71**, 429 (1982).
[56] M. Lattuada, F. Riggi, C. Spitaleri, D. Vinciguerra, and C. M. Sutera, Phys. Rev. C **26**, 1330 (1982).
[57] M. Jain, P. G. Roos, H. G. Pugh, and H. D. Holgrem, Nucl. Phys. **A153**, 49 (1970).
[58] S. Barbabino, M. Lattuada, F. Riggi, C. Spitaleri, C. M. Sutera, and D. Vinciguerra, Nuovo Cimento **53**, 327 (1979).
[59] D. R. Tilley, J. H. Kelley, J. L. Godwin, D. J. Millener, J. E. Purcell, C. G. Sheu, and H. R. Weller, Nucl. Phys. **A745**, 155 (2004).
[60] S. Barbarino, M. Lattuada, F. Riggi, C. Spitaleri, and D. Vinciguerra, Phys. Rev. C **21**, 1104 (1980).
[61] M. A. Aliotta, F. Raiola, G. Gyürky, A. Formicola, R. Bonetti, C. Broggini, L. Campajola, P. Corvisiero, H. Costantini, A. D'Onofrio, Z. Fülöp, G. Gervino, L. Gialanella, A. Guglielmetti, C. Gustavino, G. Imbriani, M. Junker, P. G. Moroni, A. Ordine, P. Prati, V. Roca, D. Rogalla, C. Rolfs, M. Romano, F. Schümann, E. Somorjai, O. Straniero, F. Strieder, F. Terrasi, H. P. Trautvetter, and S. Zavatarelli, Nucl. Phys. **A690**, 790 (2001).

[62] W. H. Geist, C. R. Brune, H. J. Karwowski, E. J. Ludwig, K. D. Veal, and G. M. Hale, Phys. Rev. C **60**, 054003 (1999).
[63] A. Krauss, H. W. Becker, H. P. Trautvetter, C. Rolfs, and K. Brand, Nucl. Phys. **A465**, 150 (1987).
[64] G. S. Chulick, Y. E. Kim, R. A. Rice, and M. Rabinowitz, Nucl. Phys. **A551**, 255 (1993).
[65] T. W. Bonner, J. P. Conner, and A. B. Lillie, Phys. Rev. **88**, 473 (1952).
[66] F. C. Barker, Nucl. Phys. **A707**, 277 (2002).
[67] P. Descouvemont, A. Adahchour, C. Angulo, A. Coc, and E. Vangioni-Flam, At. Data Nucl. Data Tables **88**, 203 (2004).
[68] G. M. Hale, document available at http://t2.lanl.gov/data/astro/astro.html
[69] K. Langanke, T. D. Shoppa, C. A. Barnes, and C. Rolfs, Phys. Lett. **B369**, 211 (1996).
[70] P. Prati, C. Arpesella, F. Bartolucci, H. W. Becker, E. Bellotti, C. Broggini, P. Corvisiero, G. Fiorentini, A. Fubini, G. Gervino, F. Gorris, U. Greife, C. Gustavino, M. Junker, C. Rolfs, W. H. Schulte, H. P. Trautvetter, and D. Zahnow, Z. Phys. A **350**, 171 (1994).
[71] S. Engstler, A. Krauss, K. Neldner, C. Rolfs, U. Schröder, and K. Langanke, Phys. Lett. **B202**, 179 (1988).